DOI: 10.1002/chem.200701813

Multifunctional Fourfold Interpenetrating Diamondoid Network: Gas Separation and Fabrication of Palladium Nanoparticles

Young Eun Cheon and Myunghyun Paik Suh*[a]

Abstract: A fourfold interpenetrating diamondoid network, $[\{[Ni(cyclam)]_2(mtb)\}_n]\cdot 8n\,H_2O\cdot 4n\,DMF$ (**1**) (MTB = methanetetrabenzoate, DMF = dimethylformamide), has been assembled from $[Ni(cyclam)][ClO_4]_2$ (cyclam = 1,4,8,11-tetraazacyclotetradecane) and methanetetrabenzoic acid (H_4MTB) in DMF/H_2O (7:3, v/v) in the presence of triethylamine (TEA). Despite the high-fold interpenetration, **1** generates 1D channels that are occupied by water and DMF guest molecules. Solid **1**, after removal of guest molecules, exhibits selective gas adsorption behavior for H_2, CO_2, and O_2 rather than N_2 and CH_4, suggesting possible applications in gas separation technologies. In addition, solid **1** can be applied in the fabrication of small Pd (2.0 ± 0.6 nm) nanoparticles without any extra reducing or capping agent because a Ni^{II} macrocyclic species incorporated in **1** reduces Pd^{II} ions to Pd^0 on immersion of **1** in the solution of $Pd(NO_3)_2\cdot 2H_2O$ in MeCN at room temperature.

Keywords: adsorption · coordination polymers · nanomaterials · palladium · redox reactions

Introduction

Porous coordination polymers (PCPs) with well-defined channels or cavities have attracted much attention because of their potential applications as new materials in gas storage,[1–5] molecular adsorption and separation processes,[6–12] ion exchange,[13,14] and heterogeneous catalysis.[15–17] In particular, redox-active porous coordination polymers are useful even though they are extremely rare, because they can oxidize or reduce certain substrates and include them in the PCPs.[9,18–20] Previously, we reported that coordination polymers incorporating Ni^{II} macrocyclic complexes produced small (<5 nm) silver and gold nanoparticles when they were immersed in Ag^I and Au^{III} solutions, respectively, owing to the redox reactions between the Ni^{II} macrocyclic species incorporated in the coordination polymers and the metal ions.[18,19] Recently, we have been interested in fabrication of palladium nanoparticles (PdNPs) in PCPs. PdNPs may enhance the hydrogen storage capacity of porous coordination polymers[21] and catalyze organic reactions.[22] Fabrication of palladium nanoparticles (1.4 ± 0.1 nm) in MOF-5, in which the $[(\eta^5\text{-}C_5H_5)Pd(\eta^3\text{-}C_3H_5)]$ complex was introduced to the MOF-5 and then reduced with H_2 gas, has been reported.[23] Although the nature of the palladium was not characterized, palladium infiltration into MOF-5 by inclusion of $[Pd(acac)_2]$ followed by reduction with H_2 gas has also been reported recently.[24]

Here, we report a new fourfold interpenetrating 3D diamondoid network, $[\{[Ni(cyclam)]_2(mtb)\}_n]\cdot 8n\,H_2O\cdot 4n\,DMF$ (**1**) (MTB^{4-} = methanetetrabenzoate, DMF = dimethylformamide), which generates 1D channels. Solid **1** exhibits selective gas sorption properties for H_2, CO_2, and O_2 rather than N_2 and CH_4. We have fabricated palladium nanoparticles (2.0 ± 0.6 nm) in the network at room temperature simply by immersion of **1** in the Pd^{II} solution without precursor compounds or reducing agents.

Results and Discussion

Preparation and X-ray structure of 1: Our design strategy was to build a 3D diamondoid network by using methanetetrabenzoate (MTB^{4-}) as a tetrahedral building block and a square-planar Ni^{II} macrocyclic complex as a linear linker (Scheme 1). Then, contrary to common coordination polymer frameworks, organic MTB^{4-} units would be located at the nodes of the diamondoid network and the Ni^{II} macrocyclic species would link them linearly. The self-assembly of

[a] Y. E. Cheon, Prof. Dr. M. P. Suh
Department of Chemistry, Seoul National University
Seoul 151-747 (Republic of Korea)
Fax: (+82) 2-886-8516
E-mail: mpsuh@snu.ac.kr

Supporting information for this article is available on the WWW under http://www.chemeurj.org/ or from the author.

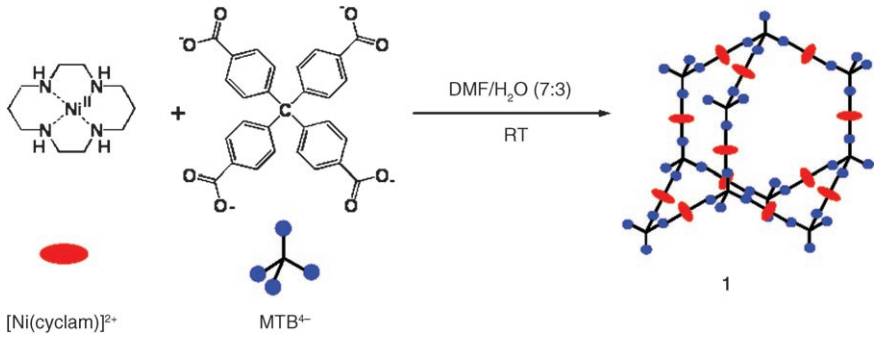

Scheme 1. Design strategy for framework **1**.

$[Ni(cyclam)]^{2+}$ and MTB^{4-} in DMF/H_2O/TEA (7:3:0.8, by vol.; TEA = triethylamine) resulted in $[\{[Ni(cyclam)]_2(mtb)\}_n]\cdot 8n\,H_2O\cdot 4n$ DMF (**1**). Solid **1** is insoluble in common solvents such as H_2O, MeOH, EtOH, MeCN, DMF, and dimethylsulfoxide.

The X-ray structure of **1** (Figure 1) shows that each MTB^{4-} binds four Ni^{II}cyclam complexes in a tetrahedral fashion with an average core angle of 106.75(25)°, and each Ni^{II} ion is coordinated with two different MTB^{4-} ligands at the axial sites to display octahedral coordination geometry, which gives rise to a diamondoid network. The adamantanoid cages of the diamondoid network have edge C···C distances of 17.1 Å and maximum pore dimensions of 33.5 Å (Figure 1a). Such large cavities induce fourfold interpenetration of the network, whose interpenetration vector runs along the *c* axis (Figure 1b). Despite the fourfold interpenetration, the structure generates 1D channels along the *c* axis. There are some examples in which open structures result despite the high-fold interpenetration,[10,25] and they sometimes provide very robust porous solids.[25a] The 1D channels are formed from repeated jar-like cavities that have a narrow entrance (2.05 × 2.05 Å) and a wider inside pocket (13.36 × 13.36 Å). The channels are filled with four DMF and eight water guest molecules per unit formula of the host, as evidenced by the IR as well as the elemental analysis and thermal gravimetric analysis/differential scanning calorimetry (TGA/DSC) data. The void space in **1** is 31.6%, as estimated by PLATON.[26]

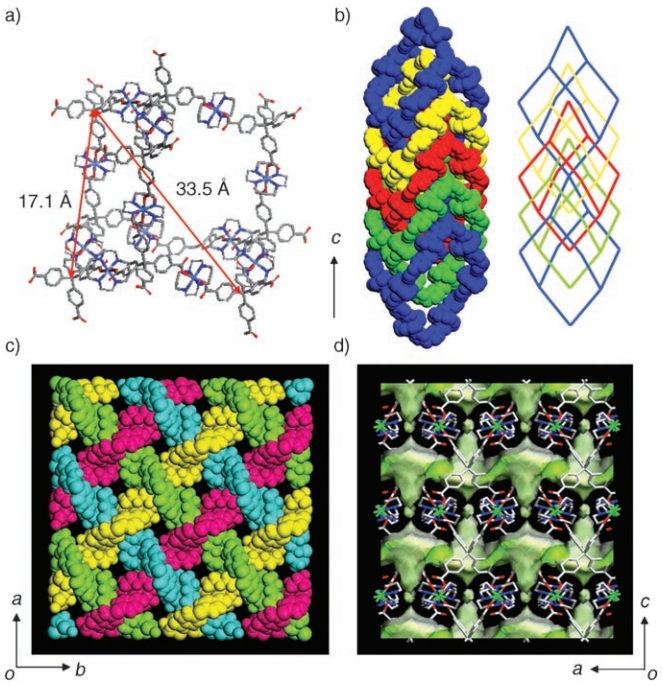

Figure 1. The X-ray crystal structure of **1**. a) An adamantanoid cage. b) Fourfold interpenetrating mode of diamondoid networks. c) View of the *ab* plane, showing that the fourfold interpenetrating networks generate 1D channels (effective window size 2.05 × 2.05 Å). Surface view seen from the *ac* plane (green: inside of pore; pale gray: pore surface).

TGA of **1** reveals a weight loss in two steps, 9.4% at 80 °C and 21.9% at 180 °C, which correspond to eight water molecules (calcd. 9.95%) and four DMF molecules (calcd. 20.2%), respectively, per formula unit (see the Supporting Information). The guest-free framework is thermally stable up to 350 °C. The crystal structure is retained up to 175 °C, as evidenced by the temperature-dependent X-ray powder diffraction (XRPD) patterns (see the Supporting Information).

When the guest molecules of **1** were exchanged with EtOH and then heated at 60 °C under vacuum for 24 h, desolvated solid **1′** resulted which had a very broad XRPD pattern. However, when **1′** was exposed to DMF/H_2O vapor (10:0.7, v/v) at 38 °C for five days, the resolvated solid (**1″**) was generated with the same XRPD pattern as **1**. There are many frameworks that collapse upon removal of guest molecules, but restore the original structure on exposure to the vapor of the guest.[7,10,27]

Selective gas sorption properties: Gas sorption was measured for desolvated solid **1′** with N_2, H_2, O_2, CH_4, and CO_2 gases. The samples for gas sorption experiments were prepared by exchange of the guest molecules of **1** with EtOH followed by removal of the EtOH. Solid **1′** does not adsorb N_2 and CH_4 gases. However, it adsorbs H_2, CO_2, and O_2 gases to show Type I isotherms, characteristic of microporous material (Figure 2a). The selective sorption of H_2, CO_2, and O_2 rather than N_2 and CH_4 gases may be attributed to the smaller kinetic diameters of H_2, CO_2, and O_2 than those of N_2 and CH_4 (H_2, 2.8; CO_2, 3.3; O_2, 3.46; N_2, 3.64; CH_4, 3.8 Å).[28] The selective sorption of CO_2 rather than N_2 gas can also be attributed to the significant quadrupole moment of CO_2 (-1.4×10^{-39} C m^2), which induces specific interactions with the host framework.[29]

Solid **1′** adsorbs H_2 gas up to 0.7 wt.% at 77 K and 1 atm (78.75 cm^3 g^{-1} at STP, 3.6 H_2 molecules per formula unit). At 77 K and 40 bar, it adsorbs H_2 gas up to 1.25 wt.% (Fig-

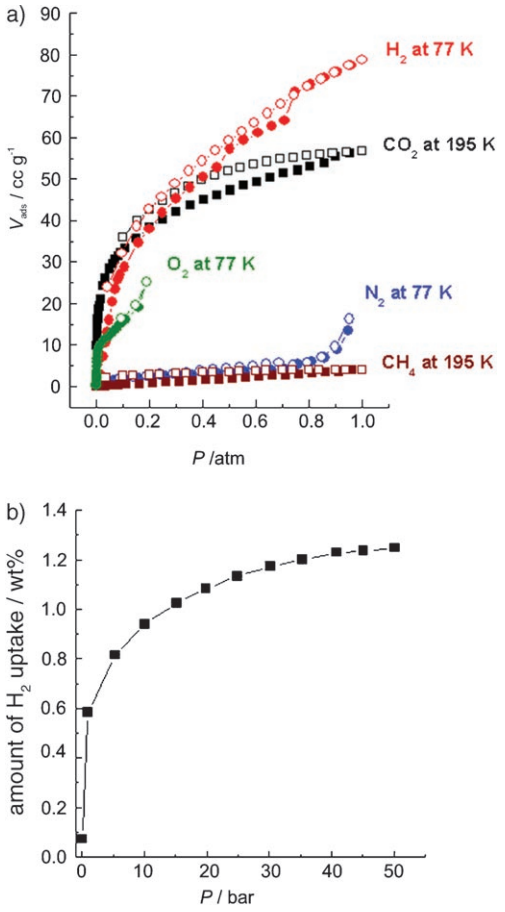

Figure 2. Selective gas sorption of **1′**. a) N_2 (blue), H_2 (red), and O_2 (green) measured at 77 K; CO_2 (black) and CH_4 (brown) at 195 K. $P_o(N_2)=760$ torr. Filled shapes: adsorption; open shapes: desorption. b) H_2 gas sorption isotherm at high pressure.

ure 2b). This H_2 adsorption capacity is much inferior to that of the MOF that we previously reported (1.9 wt.%[1a] and 2.87 wt.%[1c] at 77 K and 1 atm).

Solid **1′** also adsorbs O_2 gas up to 3.6 wt.% at 77 K and 0.19 atm (25.13 cm^{3}g^{-1} at STP, 1.1 O_2 molecules per formula unit). Since the saturation vapor pressure of O_2 is 147.8 torr at 77 K, we could not measure the O_2 sorption at higher pressures than 0.19 atm.

Solid **1′** adsorbs CO_2 gas up to 11.2 wt.% (2.53 mmol g^{-1}, 56.78 cm^{3}g^{-1} at STP) at 195 K and 1 atm (Figure 2a). The BET surface area and pore volume, 141.2 m^{2}g^{-1} (Langmuir surface area 154.2 m^{2}g^{-1}) and 0.055 cm^{3}g^{-1} respectively, were estimated from the CO_2 sorption data because **1′** does not adsorb N_2 gas. The gas sorption isotherms show hysteresis between the adsorption–desorption curves, which must be attributed to the intercrystalline voids.[30,31]

Although sorption capacities for H_2, CO_2, and O_2 are not so great as those of other MOFs, the selective gas sorption behavior of **1′** suggests that the present solid can be applied in gas separation processes: for example, for the separation of N_2 and O_2 from air, a process currently performed on a scale of billions of tons per year in the US alone, as well as for the H_2 enrichment of the N_2/H_2 exhaust mixture resulting from ammonia synthesis.

Fabrication of small palladium nanoparticles: The Ni^{II} azamacrocyclic complex coordinating anionic ligands at the axial sites can be oxidized to Ni^{III} species by the appropriate oxidizing agents.[32,33] Therefore, the coordination polymers that incorporate Ni^{II} macrocyclic species can be redox-active and react with certain metal ions. Previously we reported the reactions of redox-active coordination polymers incorporating Ni^{II} macrocyclic species with Ag^I and Au^{III} ions to produce Ag^0 and Au^0 nanoparticles, respectively.[18,19] In this study, we tried the reaction of **1** with Pd^{II} ions. The standard reduction potential in water for Pd^{II} to Pd^0 (+0.987 V versus SHE) is more positive than that (+0.799 V) of Ag^I to Ag^0.

When pale purple solid **1** was immersed in a solution of $Pd(NO_3)_2{\cdot}2H_2O$ (1.0×10^{-2} M) in MeCN at room temperature for 5 min, it turned yellow immediately. The high-resolution transmission electron microscope (HRTEM) image of the yellow solid showed the formation of Pd^0 nanoparticles, diameter 2.0 ± 0.6 nm (Figure 3). Even when the solid was immersed for 16 h, the size and shape of the nanoparticles did not change. Although the solution of $Pd(NO_3)_2$ in MeCN alone spontaneously produces nanoparticles, they have a wide size distribution (20–25 nm) and are much bigger than those produced from the reaction with **1** (see the Supporting Information). In general, the size, shape, and crystallinity of the nanoparticles depend on the concentration and counteranions of the metal ions, the temperature, and the type of solvent.[34,35] To investigate these effects, our experiments were conducted under various conditions (Pd^{II} concentration, 1.0×10^{-3}–1.0×10^{-1} M; counteranion, nitrate and acetate; temperature, room temperature to 82 °C; solvent, MeCN and acetone). The results (see the Supporting Information) indicated that these conditions did not affect the size of the nanoparticles significantly.

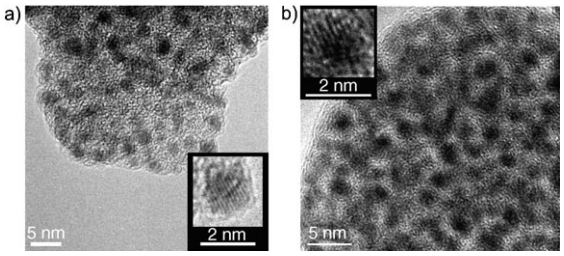

Figure 3. HRTEM images of Pd^0 nanoparticles formed by immersion of solid **1** in a solution of $Pd(NO_3)_2$ in MeCN (1.0×10^{-2} M) at room temperature: a) for 5 min (2.0 ± 0.6 nm nanoparticles); b) for 16 h.

The electron paramagnetic resonance (EPR) spectrum (Figure 4) of the resulting solid shows anisotropic signals at $g_\perp=2.175$ and $g_\parallel=2.016$, which are indicative of the tetragonally distorted Ni^{III} species,[18,19,32,33] and a peak at $g=1.992$ for Pd^0 nanoparticles. The bulk metallic state of Pd^0 is not EPR-active, but the small Pd^0 particles show a broad con-

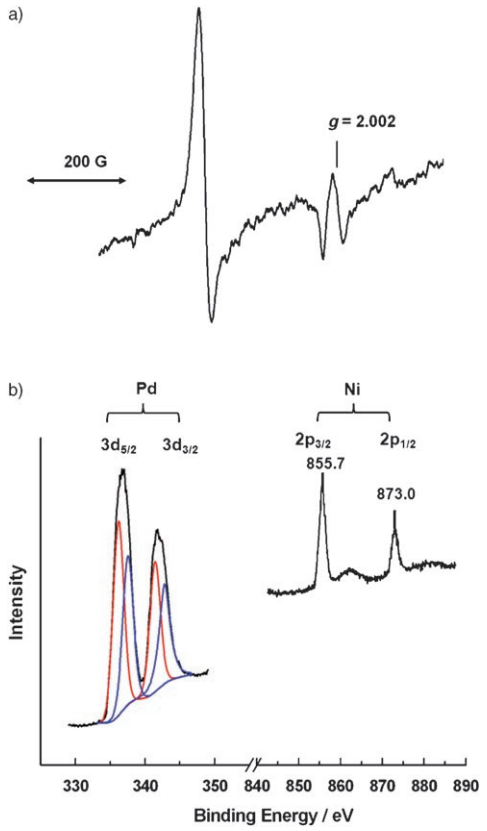

Figure 4. Spectra of the solid (powder sample) isolated after **1** was immersed in a solution of $Pd(NO_3)_2{\cdot}2H_2O$ in MeCN (1.0×10^{-2} M) for 5 min. a) EPR spectrum measured at 173 K. $g_\perp = 2.175$ and $g_\parallel = 2.016$ for Ni^{III}; $g = 1.992$ for Pd^0. b) X-ray photoelectron spectrum. Resolved peaks for Pd^{II} (337.6 and 342.7 eV) in blue and Pd^0 (336.2 and 341.5 eV) in red.

duction electron paramagnetic resonance (CEPR).[36] When the metal particles are sufficiently small, a narrowing of the CEPR line results because the average electronic energy level spacing becomes greater than the Zeeman energy and the spin relaxation processes are quenched by quantum size effects.[36]

The IR spectrum shows a peak at 1379 cm^{-1} that corresponds to free NO_3^- anions. Since the host solid becomes positively charged because of the oxidation of Ni^{II} macrocyclic species incorporated in the host solid to Ni^{III} species, it includes NO_3^- as the counteranions. The elemental analysis data indicate that Pd_2(mtb) salt was formed and mixed with the nanocomposite, owing to the partial dissociation of **1** in the $Pd(NO_3)_2$ solution, as noted in the Experimental Section. The inductively coupled plasma (ICP) results and the elemental analysis data indicate that a stoichiometric amount ($Pd^0/Ni^{III} = 1{:}2$) of palladium nanoparticles was formed from the reaction between Ni^{II} macrocyclic species of **1** and Pd^{II} ions.

X-ray photoelectron spectroscopy (XPS) and energy-dispersive X-ray spectroscopy (EDS) data indicate that Pd^{II}, Pd^0, and Ni^{III} coexist in the solid (Figure 4 and in the Supporting Information). In the XPS traces, the $2p_{3/2}$ and $2p_{1/2}$ peaks for Ni^{III} appear at 855.7 and 873 eV, respectively, which are similar to the values previously reported.[18,19] The $3d_{5/2}$ and $3d_{3/2}$ peaks of Pd^{II} appear at 337.6 and 342.7 eV and those of Pd^0 appear at 336.2 and 341.5 eV. These values are coincident with the reported values for Pd^{II} (337.8 and 343.3 eV) and Pd^0 (335.0 and 341.1 eV).[37] The peaks for Pd^{II} in XPS must be attributed to Pd_2(mtb) that is mixed with the Pd^0 nanocomposite.

When hydrogen gas was passed over the nanocomposite at room temperature for 1 h, the XPS lines of Pd^{II} moved to the lower binding energy regions (335.7 eV for $3d_{5/2}$, 341.1 eV for $3d_{3/2}$), indicating that Pd_2(mtb) was converted to Pd^0. After the hydrogen gas was passed over them, the nanoparticles became bigger and the lattice fringes become more distinct in the HRTEM images (see the Supporting Information).

The XRPD patterns (Figure 5) indicate that even after the formation of Pd^0 nanoparticles, the peaks corresponding to the (001), (200), and (201) planes of **1** are retained al-

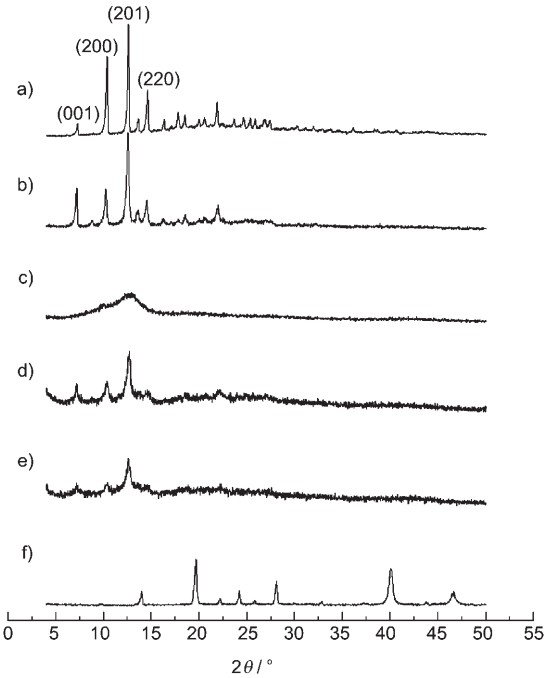

Figure 5. XRPD patterns for a) the original host framework **1**; b) guest-exchanged solid of **1** with EtOH; c) desolvated solid **1′**; d) solid isolated after immersion of **1** in a solution of $Pd(NO_3)_2{\cdot}2H_2O$ in MeCN (1.0×10^{-2} M) for 5 min; e) solid isolated after immersion of **1** in a solution of $Pd(NO_3)_2{\cdot}2H_2O$ in MeCN (1.0×10^{-2} M) for 16 h; and f) host-free palladium nanoparticles capped with PVP.

though many peaks are significantly broadened. This means that the fourfold interpenetrating 3D diamondoid structure generating 1D channels is maintained even after the network oxidation, introduction of NO_3^- anions, and formation of Pd^0 nanoparticles that are bigger than the channel apertures. We suggest the mechanism for the formation of the Pd^0 nanoparticles is such that Pd^{II} ions are introduced to the 1D channels of **1** and react with the Ni^{II} species incorporat-

ed in the host to form Pd^0 atoms, which diffuse to the surface of the solid to grow into nanoparticles. Previously, we reported that metal ions or complexes were included in the pores of the coordination polymers, and the host–guest binding constants and amounts of included metal ions depended on the size and nature of the complexes.[6,38] We also revealed that the redox-active bilayer open framework reacted with I_2 to produce a positively charged network that included I_3^- anions in the channels in a single-crystal to single-crystal manner.[9] These results support the proposition that Pd^{II} metal ions and NO_3^- ions included in the channels react with the host solid. The palladium peaks in these XRPD patterns are extremely weak, probably because the Pd^0 particles are too small and scarce compared with the host solid. Another research group also has reported that nanoparticles of Pd^0 (1.4 nm), Cu^0 (3–4 nm), and Au^0 (5–20 nm) were produced when metal precursor complexes were introduced to the 3D channels of MOF-5 with a pore size of 0.8 nm and then reduced with H_2 gas. The XRPD patterns indicated that the MOF-5 framework was retained even after the formation of nanoparticles 2–25 times bigger than the channel apertures.[23]

Host-free palladium nanocrystals capped with poly(*N*-vinyl-3-pyrrolidone) (PVP) were isolated by treatment of the Pd–host nanocomposite with H_2SO_4 (1.0×10^{-2} M) in the presence of PVP. The HRTEM image of the isolated solid indicated that 15–20 nm Pd^0 nanoparticles were formed (see the Supporting Information). The XRPD pattern (see the Supporting Information) exhibited intense peaks at $2\theta=$ 40.1, 46.7, 68.4, 82.2, and 86.9°, which were similar to the reported values (40, 46, 68, 82, and 86°) for the crystalline Pd^0.[39] The palladium dimension, which was estimated by the Scherrer equation[40] from the peak width at $2\theta=40.1°$ (Figure 5), was approximately 15 nm, coincident with the size shown in the HRTEM images (see the Supporting Information).

Increased hydrogen adsorption by palladium infiltration into MOF-5 has been reported recently, although the nature of palladium was not characterized.[24] In this case, the [Pd(acac)$_2$] complex was included in MOF-5 followed by reduction with H_2 gas. By immersion of **1** in the solution of Pd in MeCN (1.6×10^{-3} M, 8.5 mL) for 30 min, we loaded 1.0 wt.% of palladium nanoparticles into the host, and tested whether the PdNPs enhanced the H_2 adsorption capacity of **1**. However, PdNPs(1.0 wt.%)@**1** did not adsorb H_2 gas, contrary to our expectation. This must be attributed to the inclusion of NO_3^- anions that block the free space of the host solid.

Conclusion

We have assembled a new fourfold interpenetrating diamondoid network, $[\{[Ni(cyclam)]_2(mtb)\}_n]\cdot 8n\,H_2O\cdot 4n$ DMF (**1**). Despite of the high-fold interpenetration, **1** generates 1D channels. The desolvated solid of **1** exhibits selective gas sorption properties for H_2, CO_2, and O_2 rather than N_2 and CH_4 gases. These selective gas sorption properties can be applied to the separation of N_2 and O_2 from air as well as to H_2 enrichment from the N_2/H_2 mixture resulting from ammonia synthesis. Solid **1** can be also applied in the fabrication of small Pd nanoparticles ($\approx2.0\pm0.6$ nm) at room temperature simply on immersion in a solution of $Pd(NO_3)_2$ in MeCN at room temperature. Further studies on the application of the present palladium nanocomposite solid are under way.

Experimental Section

General methods: All chemicals and solvents used in the syntheses were of reagent grade and were used without further purification. MTB[41] and [Ni(cyclam)][ClO$_4$]$_2$[42] were prepared according to the methods previously reported. Infrared spectra were recorded with a Perkin–Elmer Spectrum One FT-IR spectrophotometer. UV/Vis diffuse reflectance spectra were recorded on a Perkin–Elmer Lambda 35 UV/Vis spectrophotometer. The elemental analyses and ICP-atomic emission spectroscopy were performed by the analytical laboratory in Seoul National University. TGA and DSC were performed under N_2 at a scan rate of 5 °C min^{-1} using TA Instruments TGA Q50 and DSC Q10, respectively. XRPD data were recorded on a Mac Science M18XHF-22 diffractometer at 50 kV and 100 mA for CuK_α ($\lambda=1.54050$ Å) with a scan speed of 5° min^{-1} and a 2θ step size of 0.02°. EPR spectra were recorded by using a JEOL JES-TE200. X-ray photoelectron spectra were measured by using a Sigma Probe. HRTEM images were obtained by means of a JEOL 300 kV electron microscope.

Preparation of $[\{[Ni(cyclam)]_2(mtb)\}_n]\cdot 8n\,H_2O\cdot 4n$ DMF (1): Methanetetrabenzoic acid (H_4MTB) (30 mg, 0.064 mmol) dissolved in a DMF/water/TEA mixture (2 mL:3 mL:0.08 mL) was added carefully over a solution of [Ni(cyclam)][ClO$_4$]$_2$ (60 mg, 0.130 mmol) in DMF (5 mL). The solutions were allowed to diffuse into each other at room temperature for several days. Pale purple crystals were formed, which were filtered off, washed with a DMF/water mixture, and dried briefly in air. Yield: 105 mg, 56%; FT-IR (KBr pellet): $\tilde{\nu}=3411$ (O–H), 3256 (N–H), 2925, 2862 (C–H), 1666 (O–C=O of DMF), 1592, 1546 cm^{-1} (O–C=O); UV/Vis (diffuse reflectance spectrum): $\lambda_{max}=513$ nm; elemental analysis calcd (%) for $Ni_2C_{61}H_{108}N_{12}O_{20}$: C 50.63, H 7.52, N 11.62; found: C 50.80, H 7.46, N 11.64.

Preparation of $[\{[Ni(cyclam)]_2(mtb)\}_n]\cdot 3n$ EtOH (1′): Pulverized solid **1** was immersed in EtOH (20 mL) at room temperature for 12 h. The solid was filtered and immersed in EtOH (20 mL) for another 12 h, filtered again and dried at 60 °C under vacuum for 24 h. FT-IR (Nujol mull): $\tilde{\nu}=$ 3278 (N–H), 1576, 1553 cm^{-1} (O–C=O); UV/Vis (diffuse reflectance spectrum): $\lambda_{max}=517$ nm; elemental analysis calcd (%) for $Ni_2C_{55}H_{82}N_8O_{11}$: C 57.51, H 7.20, N 9.76; found: C 57.67, H 5.92, N 9.67.

Preparation of $[\{[Ni(cyclam)]_2(mtb)\}_n]\cdot 8n\,H_2O\cdot 4n$ DMF (1″): Solid **1′** was exposed to the vapor of DMF/H_2O (10:0.7, v/v) at 38 °C for 5 days. FT-IR (KBr pellet): $\tilde{\nu}=3400$ (O–H), 3248 (N–H), 2925, 2862 (C–H), 1667 (O–C=O of DMF), 1595, 1549 cm^{-1} (O–C=O); UV/Vis (diffuse reflectance spectrum): $\lambda_{max}=521$ nm; elemental analysis calcd (%) for $Ni_2C_{61}H_{108}N_{12}O_{20}$: C 50.63, H 7.52, N 11.62; found: C 49.21, H 6.49, N 11.45.

Preparation of palladium nanocomposite: Pulverized solid **1** (144.0 mg, 0.1 mmol) was immersed in a solution of $Pd(NO_3)_2\cdot 2H_2O$ (1.0×10^{-2} M, 0.1 mmol) in MeCN (10 mL) for 5 min–16 h at room temperature. The resulting yellow solid was filtered, washed with MeCN, and dried briefly in air. Analysis calcd for the solid isolated after 5 min of immersion: $[\{[Ni^{II}(cyclam)]_2(mtb)\}_{0.4}]\cdot[\{[Ni^{III}(cyclam)]_2(mtb)\}_{0.6}](NO_3)_{1.2}\cdot 0.6\,Pd^0\cdot 0.2\,Pd_2(mtb)\cdot H_2O$; FT-IR (KBr pellet): $\tilde{\nu}=3401$ (O–H), 3234 (N–H), 2944, 2862 (C–H), 1591, 1544 (O–C=O), 1379 cm^{-1}(NO_3); UV/Vis (diffuse reflectance spectrum): $\lambda_{max}=378$ nm; elemental analysis calcd (%) for $Ni_2C_{54.8}H_{69.2}N_{9.2}O_{14.2}Pd$: C 50.33, H 5.33, N 9.85; found: C 50.86, H 5.13, N 9.67; ICP data (in HCl): concentration ratio (ppm/ppm) Pd/Ni = 36.7:40.0; molar ratio Pd/Ni = 0.51. To investigate the effect of Pd^{II} con-

centration on the size of the palladium nanoparticles, similar experiments were performed with different concentrations of $Pd(NO_3)_2 \cdot 2H_2O$ (1.0×10^{-3} M and 1.0×10^{-1} M in MeCN). To determine the effect of temperature, the experiments were also performed at 82 °C. To explore the effect of solvent, similar experiments were performed in a solution of $Pd(NO_3)_2 \cdot 2H_2O$ in acetone (1.0×10^{-3} M) at room temperature. To find the effect of the anion of the Pd^{II} salt, the experiments were also performed with $Pd(OAc)_2$ (1.0×10^{-2} M) in THF and in toluene. The results are summarized in the Supporting Information.

Preparation of host–free palladium nanoparticles: Solid **1** was immersed in a solution of $Pd(NO_3)_2 \cdot 2H_2O$ in MeCN (1.0×10^{-2} M, 10 mL) for 5 min, and then filtered. The nanocomposite solid (0.144 g) was refluxed for 2 h in EtOH/H_2O (1:1, v/v, 10 mL) in the presence of PVP and H_2SO_4 (1 mL). The solution turned yellow as the host framework was dissociated into the building blocks. Pd(pvp) nanoparticles were precipitated by the addition of diethyl ether, and isolated by filtration.

Low-pressure gas sorption studies: A measured amount of solid **1′** was introduced into a Quantachrome Autosorb-1 gas sorption apparatus, and then evacuated at 60 °C and 10^{-5} torr to remove all guest molecules. Gas sorption isotherms for N_2, H_2, and O_2 were monitored at 77 K, and those for CO_2 and CH_4 were measured at 195 K at each equilibrium pressure by the static volumetric method.

High-pressure gas sorption study: A measured amount of solid **1′** was introduced into a Rubotherm MSB (magnetic suspension balance) apparatus, and then evacuated at 60 °C under vacuum to remove all guest molecules. The data were corrected for the buoyancy of the system, sample, and adsorbate. The sample density used in the buoyancy corrections was determined from He isotherm up to 100 bar at 298 K. The gas sorption isotherm for H_2 was monitored at 77 K at equilibrium pressure up to 50 bar by the gravimetric method.

X-ray crystallography: The diffraction data were collected at 100 K with synchrotron radiation ($\lambda = 0.76000$ Å) on a 6BX Bruker Proteum 300 CCD detector with a platinum-coated double-crystal monochromator at Pohang Accelerator Laboratory (PAL), Pohang, Republic of Korea. The crystal was coated with Paraton oil to prevent loss of guest molecules. Proteum 2 (version 1.0.22)[43] was used for data collection, cell refinement, and reduction. The data were corrected for absorption. The crystal structure was solved by direct methods,[44] and refined by full-matrix least-squares refinement using the SHELXL-97 computer program.[45] The positions of all non-hydrogen atoms were refined with anisotropic displacement factors. The hydrogen atoms were positioned geometrically and refined using a riding model. The density of the disordered guest molecule was flattened by using the SQUEEZE option of PLATON.[46] The crystallographic data and selected bond distances and angles are summarized in the Supporting Information, Tables S1 and S2.

CCDC 662982 (**1**) contains the supplementary crystallographic data for this paper. These data can be obtained free of charge from The CambridgeCrystallographic Data Centre via www.ccdc.cam.ac.uk/data_request/cif.

Acknowledgements

This work was supported by the Korea Research Foundation Grant funded by the Korean Government (MOEHRD, Basic Research Promotion Fund) (KRF-2005–084-C00020), and by the SRC/ERC program of MOST/KOSEF (grant no. R11-2005-008-03002-0), Republic of Korea.

[1] a) E. Y. Lee, S. Y. Jang, M. P. Suh, *J. Am. Chem. Soc.* **2005**, *127*, 6374–6381; b) M. P. Suh, Y. E. Cheon, E. Y. Lee, *Chem. Eur. J.* **2007**, *13*, 4208–4215; c) Y. G. Lee, H. R. Moon, Y. E. Cheon, M. P. Suh, unpublished results.

[2] E. Y. Lee, M. P. Suh, *Angew. Chem.* **2004**, *116*, 2858–2861; *Angew. Chem. Int. Ed.* **2004**, *43*, 2798–2801.

[3] N. L. Rosi, J. Eckert, M. Eddaoudi, D. T. Vodak, J. Kim, M. O'Keeffe, O. M. Yaghi, *Science* **2003**, *300*, 1127–1129.

[4] B. Chen, N. W. Ockwig, A. R. Millward, D. S. Contreras, O. M. Yaghi, *Angew. Chem.* **2005**, *117*, 4823–4827; *Angew. Chem. Int. Ed.* **2005**, *44*, 4745–4749.

[5] A. G. Wong-Foy, A. Matzger, O. M. Yaghi, *J. Am. Chem. Soc.* **2006**, *128*, 3494–3495.

[6] K. S. Min, M. P. Suh, *Chem. Eur. J.* **2001**, *7*, 303–313.

[7] H. J. Choi, T. S. Lee, M. P. Suh, *Angew. Chem.* **1999**, *111*, 1490–1493; *Angew. Chem. Int. Ed.* **1999**, *38*, 1405–1408.

[8] M. P. Suh, J. W. Ko, H. J. Choi, *J. Am. Chem. Soc.* **2002**, *124*, 10976–10977.

[9] H. J. Choi, M. P. Suh, *J. Am. Chem. Soc.* **2004**, *126*, 15844–15851.

[10] H. Kim, M. P. Suh, *Inorg. Chem.* **2005**, *44*, 810–812.

[11] J. W. Ko, K. S. Min, M. P. Suh, *Inorg. Chem.* **2002**, *41*, 2151–2157.

[12] M. Eddaoudi, H. Li, O. M. Yaghi, *J. Am. Chem. Soc.* **2000**, *122*, 6834–6840.

[13] K. S. Min, M. P. Suh, *J. Am. Chem. Soc.* **2000**, *122*, 6834–6840.

[14] H. J. Choi, M. P. Suh, *Inorg. Chem.* **2003**, *42*, 1151–1157.

[15] C. D. Wu, A. Hu, L. Zhang, W. Lin, *J. Am. Chem. Soc.* **2005**, *127*, 8940–8941.

[16] K. Schlichte, T. Kratzke, S. Kaskel, *Microporous Mesoporous Mater.* **2004**, *73*, 81–88.

[17] B. Gomez-Lor, E. Gutierrez-Puebla, M. Iglesias, M. A. Monge, C. Ruiz-Valero, N. Snejko, *Chem. Mater.* **2005**, *17*, 2568–2573.

[18] H. R. Moon, J. H. Kim, M. P. Suh, *Angew. Chem.* **2005**, *117*, 1287–1291; *Angew. Chem. Int. Ed.* **2005**, *44*, 1261–1265.

[19] M. P. Suh, H. R. Moon, E. Y. Lee, S. Y. Jang, *J. Am. Chem. Soc.* **2006**, *128*, 4710–4718.

[20] S. Shimomura, R. Matsuda, T. Tsujino, T. Kawamura, S. Kitagawa, *J. Am. Chem. Soc.* **2006**, *128*, 16416–16417.

[21] a) S. Horinouchi, Y. Yamanoi, T. Yonezawa, T. Mouri, H. Nishihara, *Langmuir* **2006**, *22*, 1880–1884; b) S. Rather, R. Zacharia, S. W. Hwang, M. Naik, K. S. Nahm, *Chem. Phys. Lett.* **2007**, *438*, 78–84.

[22] a) J. Hu, Y. Liu, *Langmuir* **2005**, *21*, 2121–2123; b) S. Kidambi, J. Dai, J. Li, M. L. Bruening, *J. Am. Chem. Soc.* **2004**, *126*, 2658–2659; c) M.-K. Chung, M. Sclaf, *J. Am. Chem. Soc.* **2004**, *126*, 7386–7392; d) R. Tatumi, T. Akita, H. Fujihara, *Chem. Commun.* **2006**, 3349–3351.

[23] S. Hermes, M. K. Schroter, R. Schmid, L. Khodeir, M. Muhler, A. Tissler, R. W. Fischer, R. A. Fischer, *Angew. Chem.* **2005**, *117*, 6394–6397; *Angew. Chem. Int. Ed.* **2005**, *44*, 6237–6241.

[24] M. Sabo, A. Henschel, H. Frode, E. Klemm, S. Kaskel, *J. Mater. Chem.* **2007**, *17*, 3827–3832.

[25] a) B. Kesanli, Y. Cui, M. R. Smith, E. W. Bittner, B. Bockrath, W. Lin, *Angew. Chem.* **2005**, *117*, 74–77; *Angew. Chem. Int. Ed.* **2005**, *44*, 72–75; b) R.-Q. Zhu, Y. Yamada, Q. Xu, *Microporous Mesoporous Mater.* **2006**, *91*, 233–237; c) L.-P. Hsu, J.-Y. Wu, K.-L. J. Lu, *J. Inorg. Organomet. Polym. Mater.* **2007**, *17*, 259–265.

[26] A. L. Spek, *PLATON99, A Multipurpose Crystallographic Tool*, Utrecht University, The Netherlands, **1999**.

[27] a) H. J. Choi, M. P. Suh, *Inorg. Chem.* **1999**, *38*, 6309–6312; b) D. Maspoch. D. Ruiz-molina, K. Wurst, N. Domingo, M. Canallini, F. Biscarini, J. Tejada, C. Rovira, A. J. Veciana, *Nat. Mater.* **2003**, *2*, 190–195; c) L. Carlucci, G. Ciani, D. M. Proserpio, *Chem. Commun.* **2004**, 380–381; d) S. Ma, D. Sun, M. Ambrogio, J. A. Fillinger, S. Parkin, H.-C. Zhou, *J. Am. Chem. Soc.* **2007**, *129*, 1858–1859.

[28] D. W. Beck, *Zeolite Molecular Sieves*, Wiley & Sons, New York, **1974**.

[29] S. Coriani, A. Halkier, A. Rizzo, K. Ruud, *Chem. Phys. Lett.* **2000**, *326*, 269–276.

[30] A. Vishnyakov, P. I. Ravikovitch, A. V. Neimark, M. Bulow, O. M. Wang, *Nano Lett.* **2003**, *3*, 713–718.

[31] J. Y. Lee, J. Jagiello, *J. Solid State Chem.* **2005**, *178*, 2527–2532.

[32] M. P. Suh, *Adv. Inorg. Chem.* **1997**, *44*, 93–146.

[33] M. P. Suh, E. Y. Lee, B. Y. Shim, *Inorg. Chim. Acta* **1998**, 337–341.

[34] R. He, X. Qian, J. Yin, Z. Whu, *J. Mater. Chem.* **2002**, *12*, 3783–3786.

[35] a) H. H. Huang, X. P. Ni, G. L. Loy, C. H. Chew, K. L. Tan, F. C. Loh, J. F. Deng, G. Q. Xu, *Langmuir* **1996**, *12*, 909–912; b) M. Yamada, H. Nishihara, *Langmuir* **2003**, *19*, 8050–8056; c) L. Lu, H. Wang, Y. Whou, S. Xi, H. Whang, J. Hu, B. Zhou, *Chem. Commun.* **2002**, 144–145.
[36] a) M. Narayana, J. Michalik, S. Contarini, L. Kevan, *J. Phys. Chem.* **1985**, *89*, 3895–3899; b) J. Michalik, D. Brown, J.-S. Yu, M. Danilczyk, J. Y. Kim, L. Kevan, *Phys. Chem. Chem. Phys.* **2001**, *3*, 1705–1708; c) J. Candy, V. Perrichon, *J. Catal.* **1984**, *89*, 93–99.
[37] a) W. P. Zhou, A. Lewera, R. Larsen, R. I. Masel, P. S. Bagus, A. Wieckowski, *J. Phys. Chem. B* **2006**, *110*, 13393–13398; b) B. Richter, H. Kuhlenbeck, H.-J. Freund, P. S. Bagus, *Phys. Rev. Lett.* **2004**, *93*, 026805-1–4; c) J. C. Vedrine, M. Dufauz, C. Naccache, B. Lmelik, *J. Chem. Soc. Faraday Trans. 1* **1978**, *74*, 440–449; d) http://srdata.nist.gov/xps.
[38] H. J. Choi, T. S. Lee, M. P. Suh, *J. Inclusion Phenom. Macrocyclic Chem.* **2001**, *41*, 155–162.
[39] a) T. Teranishi, M. Miyake, *Chem. Mater.* **1998**, *10*, 594–600; b) L. Lu, H. Wang, X. Si, H. Zhang, *J. Mater. Chem.* **2002**, *12*, 156–158.
[40] C. Russel, *Chem. Mater.* **2005**, *17*, 5843–5847.
[41] a) M. Grimm, B. Kirste, H. Kurreck, *Angew. Chem.* **1986**, *98*, 1095–1099; *Angew. Chem. Int. Ed. Engl.* **1986**, *25*, 1097–1098; b) S. Dapperheld, E. Steckhan, K. G. Brinkhaus, T. Esch, *Chem. Ber.* **1991**, *124*, 2557–2567.
[42] E. K. Barefield, F. Wagner, A. W. Heilinger, A. R. Dahl, *Inorg. Synth.* **1976**, 220–225.
[43] Proteum 2 Package, Proteum 300 Area Detector Software Package, Bruker Analytical X-Ray Systems Inc., Madison, WI, USA, **2004**.
[44] G. M. Sheldrick, *Acta Crystallogr. Sect. A* **1990**, *46*, 467.
[45] G. M. Sheldrick, SHELXL97, Program for crystal structure refinement, University of Göttingen, Germany, **1997**.
[46] P. v. d. Sluis, A. L. Spek, *Acta Crystallogr. Sect. A* **1990**, *46*, 194–201.

Received: November 19, 2007
Published online: March 17, 2008

